Materials and Design 108 (2016) 440–447

Contents lists available at ScienceDirect

Materials and Design

journal homepage: www.elsevier.com/locate/matdes

Multi-phase quasicrystalline alloys for superior wear resistance

Kyungjun Lee [a], Jialin Hsu [a], Donald Naugle [b,c], Hong Liang [a,c,*]

[a] Department of Mechanical Engineering, Texas A&M University, College Station, TX 77843-3123, United States
[b] Department of Physics & Astronomy, Texas A&M University, College Station, TX, 77843, United States
[c] Department of Materials Science and Engineering, Texas A&M University, College Station, TX, 77843, United States

ARTICLE INFO

Article history:
Received 22 March 2016
Received in revised form 25 June 2016
Accepted 28 June 2016
Available online 30 June 2016

Keywords:
Multi-phase quasicrystal-based alloy
I-phase
Hardness
Friction and anti-wear
Wear mechanism

ABSTRACT

Highly wear-resistant alloys are important in many engineering and biomedical applications. In this research, a multi-phase quasicrystal-based alloy was developed using a rapid arc-melting technique. The alloy contains three characteristic phases, hard λ-$Al_{13}Fe_4$, quasicrystal icosahedral (i-phase), and ductile τ-AlCu. The Vickers micro hardness of each was 828, 795, and 552, respectively, with an overall hardness of 334 (HR15T). Due to the co-existence of these three phases, this alloy exhibits both hardness and ductility. As such, the new material has favorable wear and crack resistance. The approaches used in this study are beneficial for the future design and development of this class of quasicrystalline alloys.

1. Introduction

Since their discovery in 1984 [1], quasicrystals have attracted great interest regarding chemical catalysis, heat insulation, and surface coating applications. The unique structure of the icosahedral phase, not seen in conventional metals, leads to low thermal conductivity, absorption of infrared-light, low friction, and high hardness [2–4]. When fabricated as a coating, the combination of high hardness and low coefficient of friction improves resistance against scratches or wear [2]. Reports on use of the quasicrystalline phase in coatings are summarized in Table 1. More information about these materials can be found in the supplemental material (Table S1). As shown in the table, the most popular metallic elements are Al, Cu, and Fe. To date, there are many limitations to the application of quasicrystalline materials. For example, it has been reported that the bonding between quasicrystal coatings and the substrate is weak. Fabrication processes are usually complicated and expensive, and specifically they are difficult to fabricate over large areas. Furthermore, their poor load bearing capability can result in deflection and peeling of the coatings [5,6]. There has been increasing interest in fabrication of bulk quasicrystal-based alloys using less complicated processes with lower cost. However, quasicrystal-based alloys are known to be extremely brittle [7–9]. In this research, a simple process step was developed to fabricate bulk quasicrystal-based alloys. An arc-melting technique was selected due to its fast heating and cooling process and low cost [10]. Raw materials of aluminum, copper, and iron were used to make the quasicrystal-based alloy. These raw materials were selected because of their low toxicity, affordability, and abundance [11–17]. The quasicrystal alloy contained multiple phases: λ-$Al_{13}Fe_4$, i-phase, and τ-AlCu. This alloy has a unique combination of mechanical properties and exhibits favorable tribological performance. Detailed examination of wear was conducted, and the role of each phase in wear resistance is discussed in this manuscript.

2. Experimental details

2.1. Sample preparation

Aluminum (Al, EM Science) with purity of 99.99%, copper (Cu, J.T. Baker) with purity of 99.9%, and iron (Fe, Sigma-Aldrich) with purity of 99.98% were selected as the raw material elements. Beads of Al (65 at.%), Cu (20 at.%), and Fe (15 at.%) were mixed with the goal of making the $Al_{65}Cu_{20}Fe_{15}$ quasicrystal. This concentration was selected based on the phase diagrams in order to generate a combination of λ-$Al_{13}Fe_4$, i-phase, and τ-AlCu phases. These phases were candidates for study of wear [23,24]. An as-cast alloy was fabricated by arc-melting and quenching in the water cooled copper crucible. Detailed information is available in the supplemental information. The raw materials were put into a copper crucible in an argon-filled vacuum chamber to avoid oxidation. Then, they were melted by arc with a DC current for 60 s. After turning off the DC current, the melted material was rapidly cooled to room temperature in 5 min by the flowing cooling water around in the walls of the copper crucible. In order to improve the uniformity, the solidified sample was flipped and re-melted. This process was repeated for 8 times in order to ensure uniformity. The as-cast

* Corresponding author at: Department of Mechanical Engineering, Texas A&M University, College Station, TX, 77843-3123, United States.
E-mail address: hliang@tamu.edu (H. Liang).

http://dx.doi.org/10.1016/j.matdes.2016.06.113
0264-1275/

Table 1
Comparison of reported quasicrystalline coatings.

No.	QC Phase	Substrate	Thickness/Ra [μm]	Friction	Hardness	Wear (Load, speed, distance, temp.)	Ref.
1	$Ti_{41.5}Zr_{41.5}Ni_{17}$	Stainless steel	200/0.2	0.4	631.5 $Hv_{10\ g}$	Wear loss 6 mg (10 N, 0.5 m/s, 100 m sliding)	[18]
2	$Ti_{60}Cr_{32}Si_8$	301 Stainless steel	−/−	1	590 $Hv_{10\ g}$	Wear rate 1.1×10^{-5} mm^3/Nm (35 N, 0.001 m/s, 36 m sliding)	[19]
3	$Al_{62}Cu_{26}Fe_{12}$ (QC coating)/$Fe_{68}Al_{30}Cr_2$ (Particle)	304 Stainless steel	500/−	–	826 $Hv_{25\ g}$	Wear loss 0.027 cm^3 (87.2 N, 300 revol.)	[9]
4	$Al_{62}Cu_{26}Fe_{12}$	Mild steel	−/1.25	0.27	858 $Hv_{100\ g}$	Wear rate 9×10^{-4} g/m(20 N, 0.136 m/s, 41 m sliding)	[20]
5	$Al_{56.5}Cu_{28}Fe_{15.5}$	Inconel disk	10/0.05	0.37 (150 °C)	–	Wear rate 1.68×10^{-4} mm^3/Nm (0.98 N, 0.12 m/s, 600 m sliding, 150 °C)	[21]
6	$Al_{65}Cu_{20}Fe_{15}$	304 Stainless steel	10/0.05	0.09	1376 Hv	Scratch width 13 μm (after 50 times scratches)	[22]

alloy was then annealed in a Cress Electric furnace at 700 °C for 30 min. Detailed information is available in the supplemental material. The annealing temperature was selected to increase the amount of i-phase based on the phase diagram [25,26]. Illustration of the overall sample manufacturing process is available in supplemental information.

2.2. Characterization

The annealed alloy had a cobblestone appearance with a rough surface. Once made, the alloy was cut and mechanically polished with a polisher (STRUERS, DAP-3) for the phase analysis. Subsequently, the alloy was examined for surface morphology using an optical microscope (Keyence VHX-2000), a scanning electron microscope (SEM, VEGA3-SB), and an atomic force microscope (AFM, Nano-R™). Chemical characterization was performed through X-ray diffraction (XRD, Rigacu) and the energy-dispersive spectrum (EDS).

2.3. Mechanical testing

After annealing, both the sample and a bearing steel reference were polished for hardness measurement. The hardness values were obtained in different phases using a Vickers microhardness indenter (Tukon 1102) at 25 g-force load. Afterwards, the overall hardness of the annealed alloy and the bearing steel (using E52100 as a reference sample) was measured with a Rockwell hardness tester (Wilson 2000) with a 1/16″ ball penetrator at 15 kg applied load. For scratch tests, the surfaces of the two polished samples were cleaned with methanol and dried in an oven for 30 min. A scratch test was conducted using a tribometer (CSM Instruments) and a tungsten carbide stylus (20 μm diameter) as a counterpart. The normal loads of 1 N and 2 N were applied at a 10 mm s^{-1} scratch speed in a linear mode at room temperature. Fig. 1(a) is the schematic of the scratch test. The scratch tracks were examined using a scanning electron microscope (SEM) which detects secondary electrons and a profilometer (KLA-Tencor P-6 stylus).

2.4. Tribotests

During the scratch and wear tests, the coefficient of friction (COF) of the annealed alloy and the bearing steel sample was recorded in the computer connected to the tribometer. Similar to the scratch test, the bearing steel and the annealed alloy were polished and cleaned before the wear test. A 6 mm diameter tungsten carbide ball was used as a counterpart in a dry rotating, sliding mode as shown in Fig. 1(b). The wear tests were conducted at room temperature under the following conditions: a normal load of 5 N, sliding speed of 3 mm s^{-1}, and a total sliding distance of 25 m. A low sliding speed was selected in order to reduce the effect of heating in the contact region. A SEM and a profilometer were employed to investigate the worn surface on the wear tracks.

3. Results and discussion

3.1. Multi-phase alloy

To generate quasicyrstals, the as-cast alloy produced through arc-melting was annealed at 700 °C for 30 min. Analysis was conducted using a scanning electron microscope (SEM) and X-ray diffraction (XRD). Results in Fig. 2(a–d). Fig. 2(a–d) and S2 all show the surface of the polished annealed alloy. They have three different colors: dark gray, gray, and light gray. To identify the nature of these phase, EDS

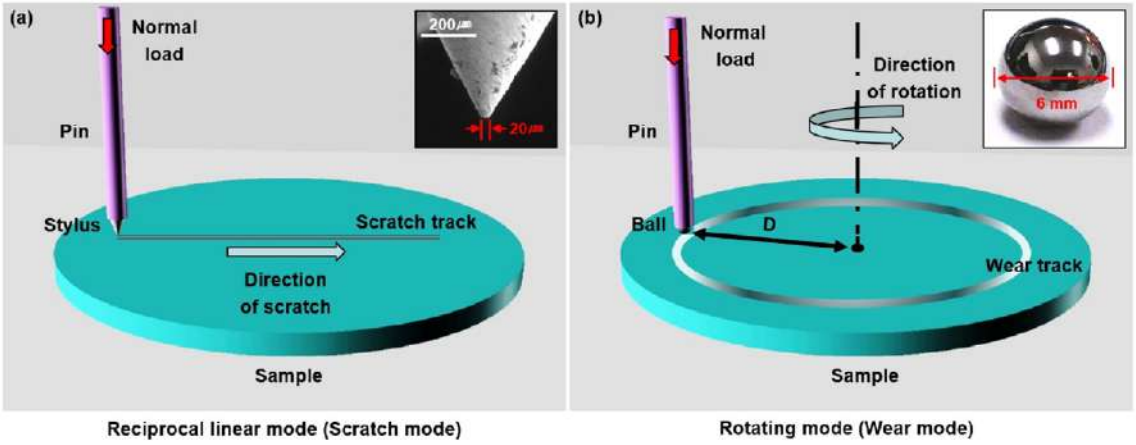

Fig. 1. Diagrams of experimental set-up. (a) a schematic of a scratch test with a 20 μm tungsten carbide shape stylus in a dry linear scratch mode and (b) a schematic of wear test with a 6 mm tungsten carbide ball in a dry rotating sliding mode at room temperature.

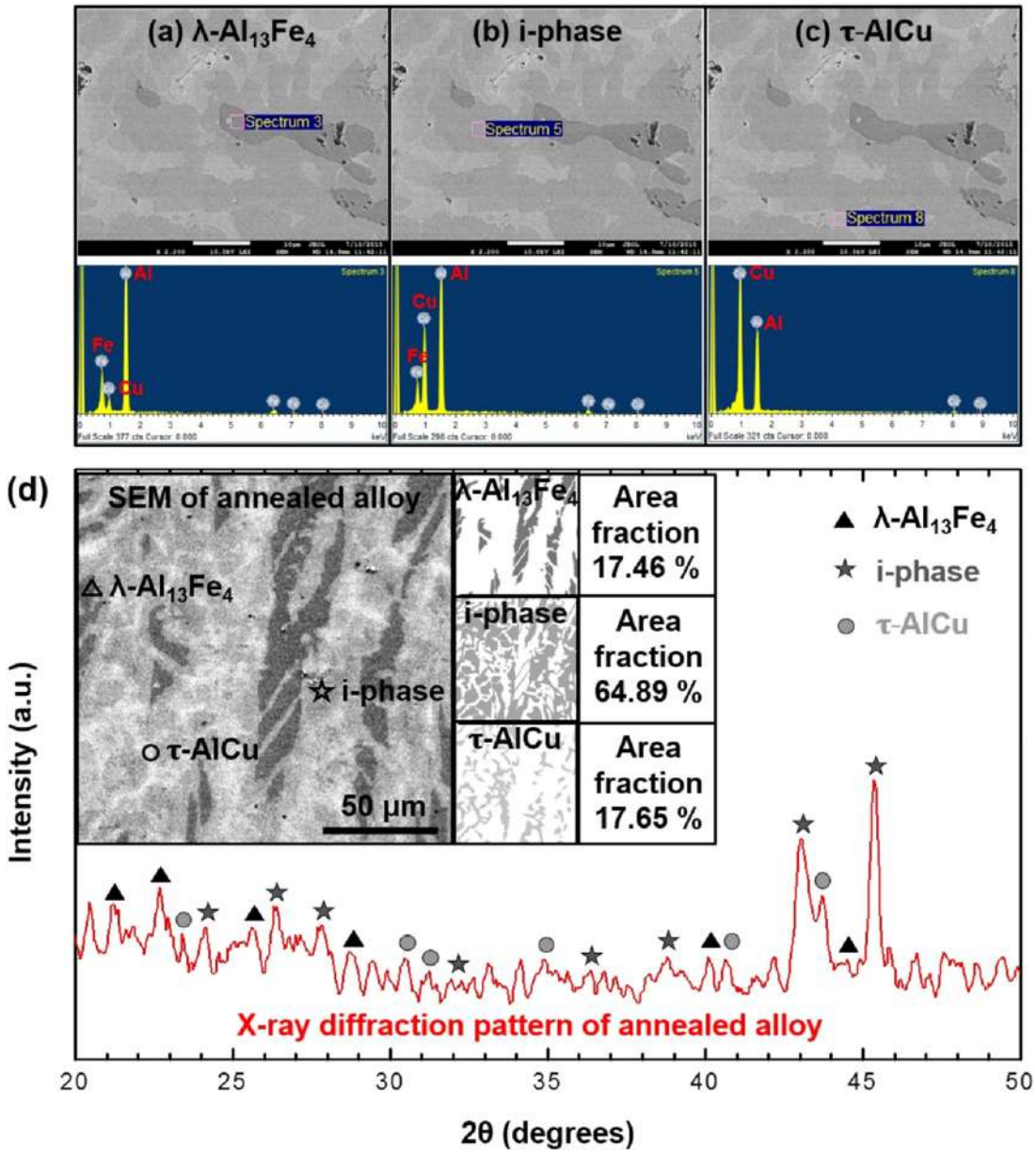

Fig. 2. EDS and XRD analysis of annealed samples. (a) EDS data of λ-$Al_{13}Fe_4$ phase, (b) EDS data of i-phase, (c) EDS data of τ-AlCu phase, and (d) spectroscopic data of XRD of an annealed alloy. Insert is the corresponding SEM image representing various phases confirmed by XRD.

was conducted in the representative areas. Results showed that each of the areas had a different concentration profile. Based on this, in combination with XRD results, we find that these three regions represent three different phases, a λ-$Al_{13}Fe_4$, an i-phase, and a τ-AlCu phase. Similar results have been previously reported [27]. Table 2 summarizes the chemical compositions of three phases shown in Fig. 2(a–c). The light gray area in the SEM image does not contain iron and thus corresponds to the τ-AlCu phase. The dark gray area represents the λ-$Al_{13}Fe_4$ phase with a small amount of copper (<6.8 at.% in EDS). The remaining gray area matches with the i-phase [16,22,28]. Thus, the annealed alloy had three distinct phases, λ-$Al_{13}Fe_4$, i-phase, and τ-AlCu. We used an image analysis method (ImageJ) to calculate the relative fraction of each phase: λ-$Al_{13}Fe_4$ covering 17.46% of the total area, i-phase at 64.89%, and τ-AlCu at 17.65%, as shown in Fig. 2(d). The volume fraction of the λ-$Al_{13}Fe_4$ is 16.21%, and that of the i-phase and the τ-AlCu are 71.18% and 12.61%, respectively, as listed in Table 3. The volume fraction was obtained through the analysis and calculation of two-dimensional images obtained using optical and SEM microscopes (refer to supplemental material). Basically, through image analysis (using image J), the grains or unit cells for each phase was determined from the change of intensity. If each unit is assumed to be a spherical grain, the diameter of the grain can be directly measured. Using this diameter, its area and volume can be calculated resulting in the area and volume fraction.

Table 2
Approximate compositions determined by EDS of each phase in the SEM micrograph obtained by secondary electrons (Fig. 2).

Location	EDS elemental composition (Atomic %)		
	Al	Cu	Fe
△ Dark gray area	59.96–62.23	5.61–6.80	31.35–34.43
☆ Gray area	48.82–54.98	24.70–28.78	18.66–20.32
○ Light gray area	44.07–68.31	31.69–50.01	0.00

3.2. Hardness

Mechanical properties are affected by each phase in the annealed alloy. The hardness of those regions in the annealed alloy were

Table 3
Microstructure analysis. Area fraction and volume fraction of each phase of the annealed alloy.

Type	Fraction values of each phase (%)		
	λ-$Al_{13}Fe_4$	i-phase	τ-AlCu
Area fraction	17.46	64.89	17.65
Volume fraction	16.21	71.18	12.61

measured using a Vickers micro-indenter. They ranged from 482 Hv to 912 Hv on various indents (Fig. 3(a)). The hardness of the λ-$Al_{13}Fe_4$ phase had an average value of 828 Hv and ranged from 740 Hv to 912 Hv. The quasicrystal i-phase had an average hardness of 795 Hv, ranging from 702 Hv to 863 Hv. The τ-AlCu phase average was 552 Hv (482–601 Hv). Their value ranking is: λ-$Al_{13}Fe_4$ > i-phase > τ-AlCu. In addition, each phase in the annealed alloy exhibited much higher hardness than that of their elements as raw materials, i.e., Al (32 Hv), Cu (70 Hv), and Fe (115 Hv). The hardness measured using a Rockwell hardness tester had a value of 334 HR15T (ranging from 219 to 561 HR15T), as shown in Fig. 3(b). This is because of the presence of λ-$Al_{13}Fe_4$ and icosahedral phase that made up the majority portion of the annealed alloy. It is noted that the overall hardness of the annealed alloy was about 3.65 times higher than that of the bearing steel reference (88.8 HR15T). The comparison is available in Fig. 3(b) and in supplemental information. The hardness of the multi-phase alloy with the i-phase is about 12.3 times higher than an Al 6061 alloy reference (0.6 GPa) [10].

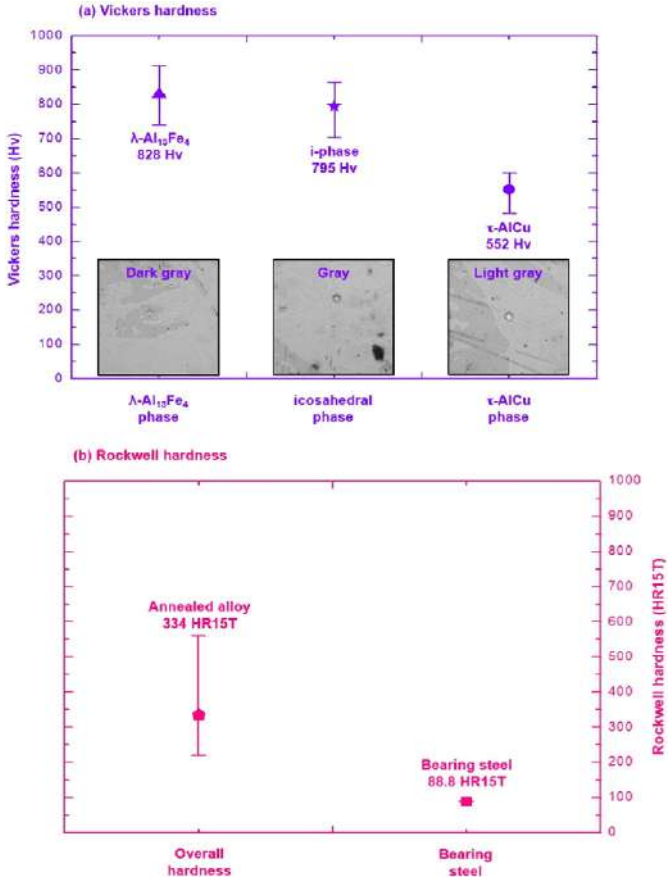

Fig. 3. Characteristic of mechanical properties of an annealed alloy (a) Vickers hardness values of: λ-$Al_{13}Fe_4$ phase having dark gray is approximately 828 Hv, the hardness of the i-phase having gray is about 795 Hv, and the hardness of τ-AlCu phase approximately 552 Hv and (b) Rockwell hardness values of an annealed alloy and bearing steel. Overall hardness of an annealed alloy is about 334 HR15T and a bearing steel has about 88.8 HR15T.

3.3. Tribological performance

3.3.1. Frictional performance

The coefficient of friction (COF) of two samples (a bearing steel reference and the annealed alloy) against a tungsten carbide ball is shown in Fig. 4(a). For the bearing steel, the average value of COF was 0.389 with a range between 0.059 and 0.498. Its COF increased steadily due to running in. Then the COF was stabilized. The annealed alloy showed an average COF of 0.076 with COFs ranged in 0.029–0.165. The COF was approximately 5 times lower in comparison with the reference sample. As noted above, this sample contains more than 60% of quasicrystal i-phase and around 17% of the ductile τ-AlCu phase. It is reported that the i-phase provides low friction [29]. The ductile phase is expected to exhibit low friction as well. It's most likely that the low friction found in our alloy was primarily due to those two phases.

3.3.2. Anti-wear behavior

The profiles of the worn surfaces were measured to assess wear. Fig. 4(b–e) show the scanning electron microscope images and surface profiles of two samples, the bearing steel reference and the annealed alloy. The bearing steel was tested against a tungsten carbide ball (diameter 6 mm) slide for 5 and 25 m under a normal load of 5 N. The result (Fig. 4(b)) shows the wear track had a depth of 0.59 μm and a width of 102.37 μm after a 5 m sliding distance. As the sliding distance reached 25 m, the depth and width of the wear track were increased to 1.40 μm and 225.49 μm, respectively in Fig. 4(d). In contrast, when the annealed alloy was slid against the tungsten carbide ball, relatively shallow and narrow tracks were observed (Fig. 4(c, e)). Wear tracks of the bearing steel and the annealed alloy were examined using an SEM to investigate the wear mechanisms, and the results are shown in Fig. 4(f, g). Fig. 4(f) shows the wear track of the bearing steel, and the right figure (Fig. 4(g)) shows the wear track of the annealed alloy. In Fig. 4(f), there is an area showing adhesive wear (inside the blue dashed ellipse). Close to the edge of the wear track, there were groves along the sliding direction, indicating abrasive wear. In contrast to this, in the case of the annealed alloy in Fig. 4(g), a few smooth grooves parallel to the sliding direction were observed on the wear track, which indicates abrasion. There were also areas (the red dashed ellipse) showing a layer-like feature of adhered debris in Fig. 4(g). Here, wear volumes of the two samples were calculated by multiplying the cross sectional area of wear track and the total sliding distance. The comparison of wear volumes and specific wear rates is shown in Table 4 and Fig. 4(h). The annealed alloy indicated significantly higher wear resistance. We noticed that there was no measurable wear on the tungsten carbide ball (Fig. 4(i)). This is due to its high hardness (~1500 Hv) in comparison to that of the annealed alloy (912 Hv).

3.4. Improved scratch resistance

A scratch test was conducted. The profiles of the scratched surfaces from the bearing steel (reference) and the annealed alloy were obtained using a profilometer. Fig. 5(a–f) show scratch tracks and profiles for them. For the bearing steel under 1 N normal load, a depth of 7.80 μm and a width of 49.52 μm were exhibited. On the other hand, the annealed alloy under 1 N normal load showed 2.01 μm depth and 20.23 μm width. Under 2 N normal load, the wear track of the bearing steel had a depth of 11.8 μm and width of 75.85 μm (Fig. 5(c)). The annealed alloy only had a depth of 5.25 μm and a width of 41.32 μm. (Fig. 5(d)). The scratch track of the bearing steel was 4 times deeper and 2.5 times wider than that of the annealed alloy containing the quasicrystal. This indicates that the annealed alloy possesses a much higher scratch resistance. To further understand this, scratch tracks were studied using the scanning electron microscope. In the case of the bearing steel, a large amount of materials piled up on both sides of the scratch. This was due to the softness of the bearing steel. See Fig. 5(b, d) which show the abrasive wear. The areas in blue circles display that the

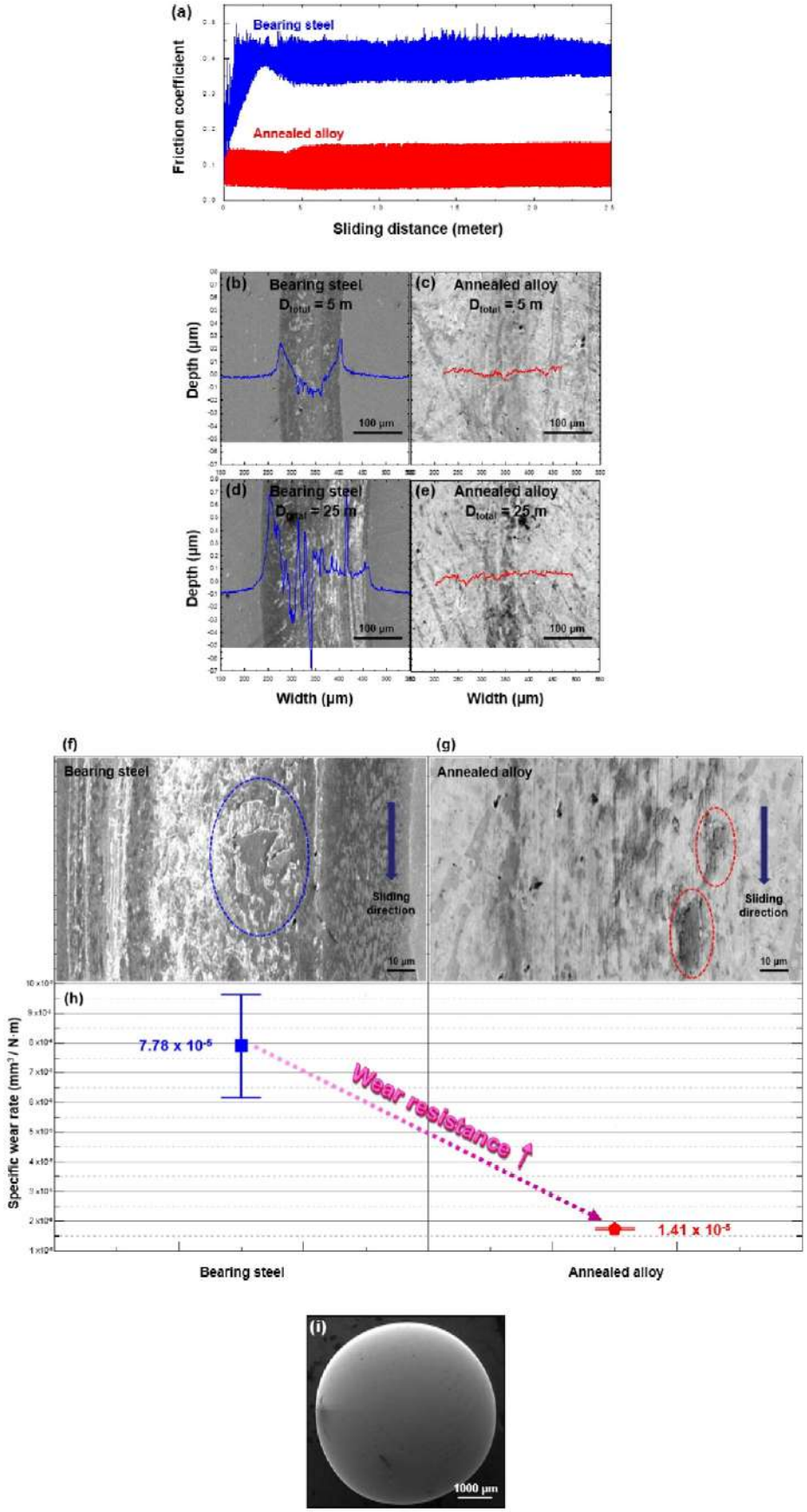
(a)
Bearing steel
Annealed alloy
Friction coefficient
Sliding distance (meter)
(b) Bearing steel
D_total = 5 m
(c) Annealed alloy
D_total = 5 m
(d) Bearing steel
D_total = 25 m
(e) Annealed alloy
D_total = 25 m
Depth (μm)
100 μm
Width (μm)
(f)
Bearing steel
Sliding direction
10 μm
(g)
Annealed alloy
(h)
7.78 x 10⁻⁵
Wear resistance ↑
1.41 x 10⁻⁵
Specific wear rate (mm³ / N·m)
Bearing steel
Annealed alloy
(i)
1000 μm

Table 4
Tribological performance analysis. Wear volume losses of the bearing steel and the annealed alloy.

Materials	Wear volume (μm^3)		
	Min.	Ave.	Max.
Bearing steel	7.80×10^6	9.73×10^6	11.42×10^6
Annealed alloy	1.72×10^6	1.76×10^6	1.79×10^6

materials were almost peeled off (Fig. 5(e)). This phenomenon was recognized to be adhesive wear. Abrasive and adhesive wear were simultaneously observed in the scratch track of the bearing steel. As a result, the bearing steel exhibited severe damage. However, the annealed alloy containing the quasicrystal exhibited a shallow scratch scar as shown in the right figure, Fig. 5(f). Therefore, the annealed alloy has significantly better scratch resistance properties than the bearing steel.

As discussed earlier, the annealed alloy had a few shallow grooves on the wear track (Fig. 4(g)). There was no crack found. This sample had a relatively ductile phase of τ-AlCu, as shown in Fig. 2. This phase was abraded through sliding due to plastic deformation forming grooves, as seen in the light gray areas of the SEM image (Fig. 4(g)). The dark areas associated with the λ-$Al_{13}Fe_4$ phase exhibited steps indicating elevated surfaces. This means that this phase is harder with less wear (Fig. 4(h)). Fig. 6(a, b) are illustrations of the surface morphology of the annealed alloy. The scratch track shown in Fig. 6(c) is correlated with a high COF. This high COF is due to the hard λ-$Al_{13}Fe_4$ phase and the ductile τ-AlCu phase. Based on the above observations, a comprehensive diagram showing the competing wear mechanisms for the three different phases was generated, as shown in Fig. 6(d). The bulk multi-phase alloy contains three phases (λ-$Al_{13}Fe_4$, i-phase (quasicrystals), and τ-AlCu) which result in the increased wear resistance. The mechanisms are attributed to those three phases. The λ-$Al_{13}Fe_4$ phase which has the highest hardness is favorable to wear resistance. The i-phase also has a relatively high hardness that contributes to increased wear resistance and is also considered to provide low friction [2–4]. The τ-AlCu phase is soft that promoted the increase in toughness (reference to supplemental material). The toughness was calculated using the method described in reference [30]. As a result, this three-phase alloy exhibits increased toughness, as demonstrated by the SEM image of the scratch track where there were no cracks (Fig. 5(f)).

4. Conclusions

A bulk Al-Cu-Fe quasicrystal-based alloy was developed using an arc-melting method. This alloy contains three phases, λ- $Al_{13}Fe_4$, quasicrystalline i-phase, and τ-AlCu. The hardness of the alloy is 334 HR15T, 3.65 times higher than the bearing steel (88.8 HR15T) and 12.3 times higher than that of a comparable aluminum alloy (Al 6061, 0.6 GPa). The friction coefficient of the alloy is steady at around 0.076, which was 5 times lower than that of the bearing steel. The wear rate of the multi-phase quasicrystal-based alloy is 1.418×10^{-5} $mm^3/N \cdot m$, around 5.53 times below that of conventional steels. The alloy has an overall increased fracture toughness.

Future work will focus on developing a predictive model to quantitatively evaluate the contribution to the wear of each phase.

Acknowledgments

Authors thank Dr. Daya Rathnayaka for assistance with the arc-melter. They wish to acknowledge the assistance of M. Fevzi Ozaydin, Wei Dai, Hyunho Choi, and Lian Ma in data collection. DGN acknowledges the support of the Robert A. Welch Foundation, Houston, TX (Grant No. A-0514). This work was partially supported by the Turbomachinery Research Laboratory at the Texas A&M University.

Appendix A. Supplementary data

Supplementary data to this article can be found online at http://dx.doi.org/10.1016/j.matdes.2016.06.113.

References

[1] D. Shechtman, Metallurgical transactions. A, Phys.Metall. Mater.Sci. 15 (1984) 1987–1997.
[2] Y. Zhang, S. Yu, Y. Luo, H. Hu, Mater. Sci. Eng. A 472 (2008) 59–65.
[3] P. Brunet, L.M. Zhang, D.J. Sordelet, M. Besser, J.-M. Dubois, Mater. Sci. Eng. A 294–296 (2000) 74–78.
[4] J.-M. Dubois, Mater. Sci. Eng. A 294–296 (2000) 4–9.
[5] S.J. Bull, Surf. Coat. Technol. 50 (1991) 25–32.
[6] S.J. Bull, E.G. Berasetegui, Tribol. Int. 39 (2006) 99–114.
[7] X. ZHOU, Trnas. Nonferrous MEt. Soc. 14 (2004) 464–469.
[8] X. ZHOU, J. Mater. Sci. Technol. 20 (2004) 709–713.
[9] D.J. Sordelet, M.F. Besser, J.L. Logsdon, Mater. Sci. Eng. A 255 (1998) 54–65.
[10] M.F. Ozaydin, H. Liang, J. Tribol. (2015).
[11] E. Huttunen-Saarivirta, J. Alloys Compd. 363 (2004) 154–178.
[12] P. Barua, B.S. Murty, B.K. Mathur, V. Srinivas, J. Mater. Res. 17 (2011) 653–659.
[13] V.V. Cherdyntsev, S.D. Kaloshkin, I.A. Tomilin, E.V. Shelekhov, A.I. Laptev, A.A. Stepashkin, V.D. Danilov, Phys. Metals Metallogr. 104 (2007) 497–504.
[14] U. Köster, W. Liu, H. Liebertz, M. Michel, J. Non-Cryst. Solids 153–154 (1993) 446–452.
[15] L. LityŃSka-DobrzyŃSka, J. Dutkiewicz, K. Stan-GŁOwiŃSka, L. Dembinski, C. Coddet, P. Ochin, Acta Physica Polonica A. 126 (2014) 512–515.
[16] C.L. Chien, M. Lu, Phys. Rev. B 45 (1992) 12793–12796.
[17] M. GÖĞEbakan, B. Avar, O. Uzun, Mater. Sci. 27 (0137–1339) (2009) 919–926.
[18] P.P. Bandyopadhyay, S. Siegmann, Surf. Coat. Technol. 197 (2005) 1–9.
[19] M. Hadad, P.P. Bandyopadhyay, J. Michler, J. Lesage, Wear 267 (2009) 1002–1008.
[20] W.D. Yuan, T.M. Shao, E. Fleury, D. Se, D.R. Chen, Surf. Coat. Technol. 185 (2004) 99–105.
[21] B.S. Phillips, J.S. Zabinski, Tribol. Lett. 15 (2003) 57–64.
[22] Y. Ding, D.O. Northwood, A.T. Alpas, Surf. Coat. Technol. 96 (1997) 140–147.
[23] V. Raghavan, J. Phase Equilib. Diffus. 31 (2010) 449–452.
[24] E.P. Georgiou, S. Achanta, S. Dosta, J. Fernández, P. Matteazzi, J. Kusinski, R.R. Piticescu, J.P. Celis, Appl. Surf. Sci. 275 (2013) 142–147.
[25] P. Barua, B.S. Murty, B.K. Mathur, V. Srinivas, J. Appl. Phys. 91 (2002) 5353.
[26] T. Grenet, F. Giroud, C. Loubet, J.L. Joulaud, M. Capitan, Mater. Sci. Eng. A 294 (2000) 838–841.
[27] D.A. Shulyatev, A.S. Nigmatulin, M.A. Chernikov, M.V. Klyueva, D.S. Shaitura, E.A. Golovkova, Acta Physica Polonica, A. 126 (2014) 581–584.
[28] M. Lu, C.L. Chien, Hyperfine Interact. 71 (1992) 1525–1529.
[29] D.S. Shaĭtura, A.A. Enaleeva, Crystallogr. Rep. 52 (2007) 945–952.
[30] A.G. Evans, E.A. Charles, J. Am. Ceram. Soc. 59 (1976) 371–372.

Fig. 4. Friction and wear of a bearing steel and the annealed alloy. (a) variations of the coefficient of the friction at 5 N normal load under rotating mode with 6 mm tungsten carbide ball as a counterpart: a COF of a bearing steel (blue line) and a COF of the annealed alloy (red line), SEM micrographs (through secondary electrons) and profiles of wear tracks: (b) a bearing steel (top left) and (c) the annealed alloy (top right) at a total sliding distance of 5 m. And (d) a bearing steel (bottom left) and (e) the annealed alloy (bottom right) at a total sliding distance of 25 m. Enlarged SEM image of wear scar: (f) a bearing steel and (g) the annealed alloy. (h) specific wear rate of two samples: a bearing steel having 7.78×10^{-5} $mm^3/N \cdot m$ specific wear rate (left) and the annealed alloy having 1.41×10^{-5} $mm^3/N \cdot m$ specific wear rate (right). (For interpretation of the references to color in this figure legend, the reader is referred to the web version of this article.)

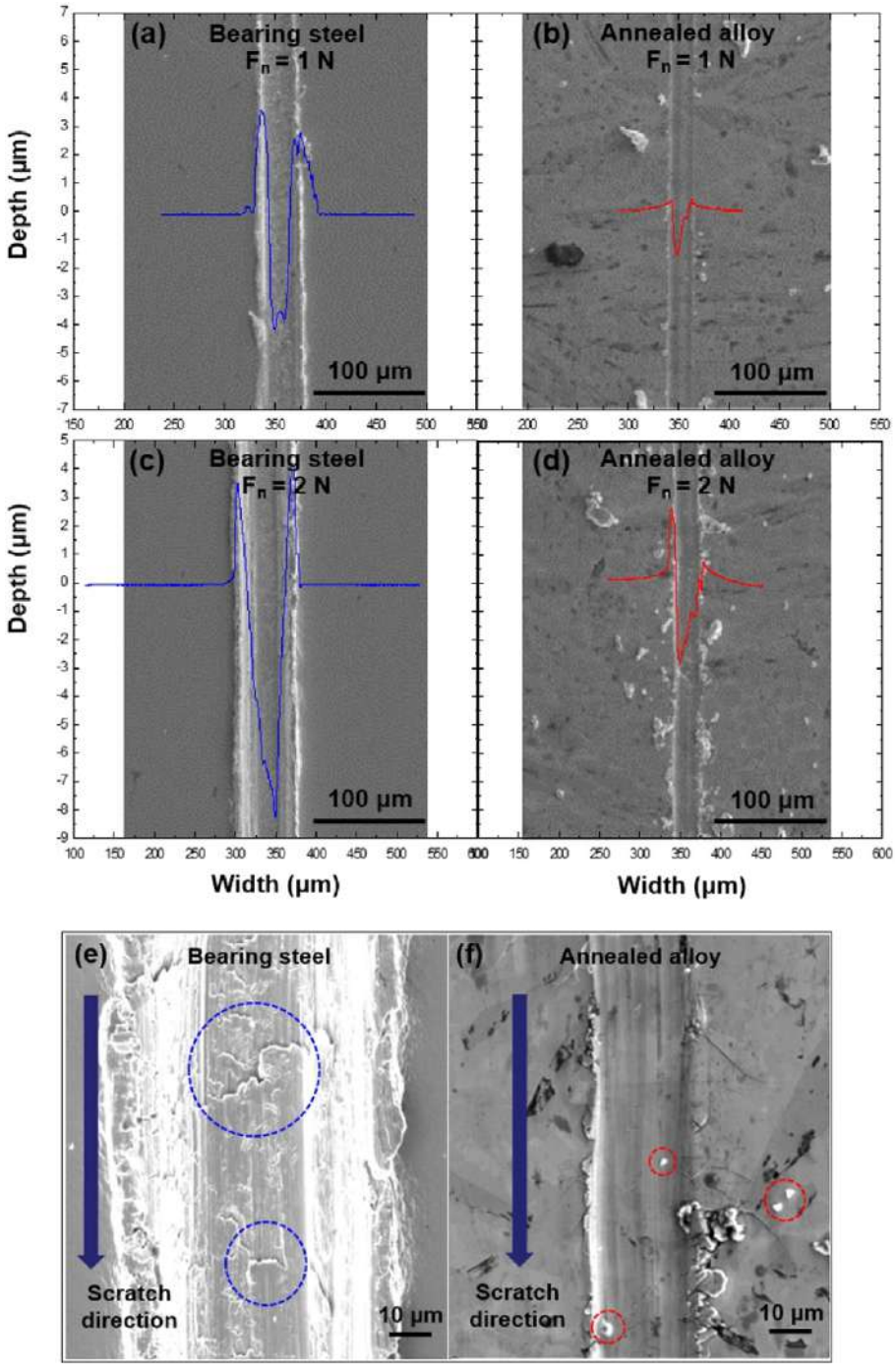

Fig. 5. SEM micrographs and profiles of scratch tracks produced by 1 N and 2 N normal loads during scratch testing. SEM micrographs and profiles of scratch tracks after scratch testing: (a) a bearing steel and (b) an annealed alloy at 1 N normal load and (c) a bearing steel and (d) the annealed alloy at 2 N normal load. High magnification SEM images of scratch tracks: (e) a bearing steel (left) and (f) the annealed alloy (right).

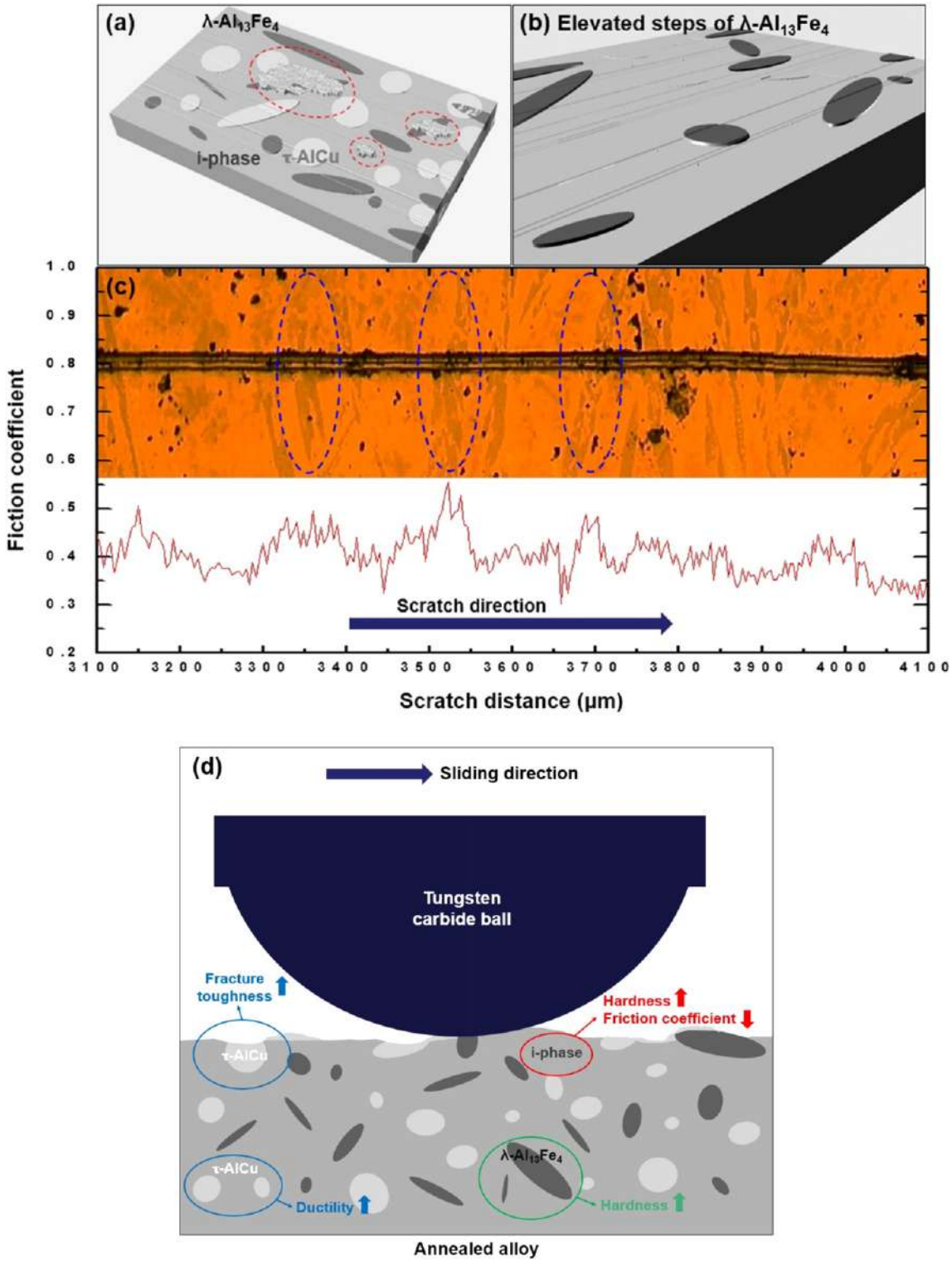

Fig. 6. Proposed mechanism of the designed alloy. (a) Illustration of a surface morphology of the annealed alloy after wear testing and (b) illustration showing elevated steps of λ- $Al_{13}Fe_4$ phase. (c) An optical microscope image of a scratch track is matched with the COF of the annealed alloy. (d) A proposed mechanism of a bulk multi-phase alloy containing λ-$Al_{13}Fe_4$ phase, i-phase (quasicrystals), and τ-AlCu showing increased wear and crack resistance.